



# Influence of mortars comprised of manufactured sand with offshore sand on the performance of masonry and brick–mortar joint

Branavan Arulmoly<sup>1</sup> · Chaminda Konthesingha<sup>1</sup> · Anura Nanayakkara<sup>2</sup>

Received: 28 June 2021 / Accepted: 5 February 2022  
© Springer Nature Switzerland AG 2022

## Abstract

Emerging environmental problems are identified due to the improper sand extraction near the riverbeds for the construction activities. This research was involved with completely replacing river sand by alternatives in masonry works. Manufactured sand and offshore sand were utilized as the substitutions for river sand and incorporated in mortars in the forms of manufactured sand alone and blending of both alternatives. Cement–sand and lime–cement–sand mortars were prepared to fabricate the masonry specimens and brick–mortar joints. The mechanical characteristics of masonry and brick–mortar joints were investigated using the available standards. The compressive and flexural strengths of masonry were greatly improved by the mortars included manufactured sand alone and the blended sand mortars. The diagonal tensile strength of masonry with the alternatives showed conflicting trends. Shear and adhesive strengths of brick–mortar joint were significantly advanced by the alternative mortars. Fine aggregate properties such as angularity, surface roughness and packing density were correlated with the masonry properties and some models were proposed to evaluate the rationale behind these effects.

**Keywords** Masonry · Brick–mortar bond · Manufactured sand · Offshore sand · Mechanical properties

## Abbreviations

RS	River sand
MS	Manufactured sand
OS	Offshore sand
CM	Cement–sand mortar
LCM	Lime–cement–sand mortar
$f_A$	Angularity index of fine aggregate
$f_i$	Surface roughness index of fine aggregate
$\rho$	Packing density of fine aggregate
$f_{cm}$	Compressive strength of mortar
$f_{lm}$	Flexural strength of mortar
$f'_m$	Compressive strength of masonry
$S_s$	Diagonal tensile/shear strength of masonry

$R_t$	Modulus of rupture parallel to bed joints
$R_u$	Modulus of rupture perpendicular to bed joints
$\tau_s$	Shear strength of brick–mortar bond
$\delta_A$	Adhesive strength of brick–mortar bond

## Introduction

Masonry is a composite, individual structural unit, which is an assemblage of bricks or blocks and mortar. The use of masonry for construction has been in practice since many centuries, due to its various beneficial properties for long-term operations [1]. Masonry structures are made with low-cost materials which have high compressive strength, good soundness, better thermal insulation characteristics and high durability [2]. The strength of masonry is influenced by several factors including the mortar strength. The primary function of mortar in masonry is it being a medium which binds the individual walling units together to form a continuous structure. Therefore, mortar should have enough bearing resistance to withstand the stresses transferring through the walling units. However, there are also some other properties that the mortar should comply for the ease of construction and maintenance [1, 3]. For instance, mortars must

✉ Branavan Arulmoly  
branavanarulmoly@sjp.ac.lk

Chaminda Konthesingha  
konthesingha@sjp.ac.lk

Anura Nanayakkara  
sman@civil.mrt.ac.lk

<sup>1</sup> Department of Civil Engineering, University of Sri Jayewardenepura, Mt. Lavinia 10390, Western Province, Sri Lanka

<sup>2</sup> Department of Civil Engineering, University of Moratuwa, Moratuwa 10400, Western Province, Sri Lanka

be workable for easy spreading and applying, should have enough workable life and water retention capacity, etc. [4].

The above-mentioned properties of mortar depend on the constituents such as cement, fine aggregate and admixtures. Fine aggregate plays the major role in mortar as it is the only aggregate which contributes around 60–70% of the total volume [5]. Currently, the construction industries from developed and developing countries erect large-scale as well as small-scale masonry structures to fulfill the infrastructure requirements. River sand has been utilized as the conventional fine aggregate in most of the countries for the masonry works [6]. This has raised a question on the continuous usage of river sand for masonry constructions due to the increased environmental drawbacks. Some researchers have proved various adverse impacts to the ecology of environment as a result of the continual over-extraction of sand near the riverbeds [7–10]. Researchers are now seeking different alternatives for partially replacing river sand for the mortar production to overcome the escalated demand for river sand. The studies executed by Gonçalves et al. [11], Cortes et al. [12] and Guifeng et al. [13] revealed that the strength of mortar was greatly increased when manufactured sand was used as a partial replacement for river sand. Less number of literatures are available on investigating the properties of mortar containing the marine sediments such as offshore sand and sea sand. Aoual-Benslafa et al. [14], De Schutter and Poppe [15] and Manjunath et al. [16] investigated the characteristics of mortars prepared with sea sand. Authors identified that the fresh properties of mortars were considerably improved with the sea sand inclusion as a partial replacement for river sand. Based on the literature review, manufactured sand and offshore sand were deemed as the better alternatives for river sand to improve both hardened and fresh properties of mortars.

A considerable number of studies have been executed on the mechanical properties of unreinforced masonry and brick–mortar bond. Malyszko [17] studied the in-place shear and tensile strength of small brickwork specimens. The authors found three different failure modes such as shear slip along bed joints, diagonal tensile cracking and shear compression failure from the diagonal compression test. Costigan et al. [18] evaluated the predicted models on the mechanical behavior of unreinforced lime-mortar masonry under compression. The study concluded some nonlinear relationships between the stress–strain behavior of masonry and the strength of mortar. Dehghan et al. [19] analyzed the mechanical properties of masonry with different sand grading. It was observed that the finer sand in mortars declined the compressive strength, elastic modulus and bond strength

than the coarser sand. Also, the authors found that the mechanical properties of lime–cement–sand mortar were more sensitive to the sand grading than the cement–sand mortars. Furthermore, Pavia and Hanley [20] investigated the flexural bond strength of hydraulic lime mortar and clay brick. The flexural bond strength was examined using a bond wrench test with five different lime mortars with a specific flow. Thaickavil and Thomas [21] carried out a case study on the cracking behavior and the compressive strength of masonry prisms. The brick type, masonry strength and height-to-thickness ratio of masonry prisms were selected as the design parameters for the experimental analysis. The authors suggested that the predicted models were complied with the experimental results. In addition to the above-mentioned literatures, some more studies are also available regarding the mechanical behavior of masonry and brick–mortar bond [22–27].

## Research gap and significance

A considerable number of studies have already been established on investigating the properties of mortar comprising manufactured sand and marine sediments as the alternatives for partially replacing river sand. A key investigation related to the present study can be found in the literature made by Arulmoly et al. [28] and Arulmoly et al. [29] where the authors checked fluid and stiffened performance of cement–sand and lime–cement–sand mortars, respectively, made with manufactured sand and offshore sand and some positive outcomes were concluded with the selected alternatives. Furthermore, plenty of literatures reported the behavior of unreinforced masonry and brick–mortar joint with different design parameters. However, none of literatures are involved with analyzation of the effects of replacing river sand with either manufactured sand or offshore sand on the behavior of unreinforced masonry and brick–mortar joint. Therefore, this study contemplates the influence of complete replacement of river sand with manufactured sand alone and blending of manufactured sand with offshore sand in both cement–sand and lime–cement–sand mortars on the performance of masonry and brick–mortar bond.

It is true that the river sand mining problem has exceeded the limit in some Asian, European and African countries [30, 31]. This requires an immediate solution for the construction industries to control or cease the escalated river sand mining. By utilizing proper river sand substitutions in the masonry works, this emerging problem can be solved to an extent. Hence, a complete

**Table 1** Properties of cement conforming to EN 197-1 [32] and SLS 107 [33]

Property	Selected cement	Standard limitations
Compressive strength (2 days)	> 25 N/mm <sup>2</sup>	≥ 10 N/mm <sup>2</sup>
Compressive strength (28 days)	> 52 N/mm <sup>2</sup>	42.5–62.5 N/mm <sup>2</sup>
Setting time	130–150 min	≥ 60 min
Fineness	330–340 m <sup>2</sup> /kg	Not defined
Soundness	< 1 mm	≤ 10 mm
Relative density	~ 3.08	Not defined
Sulfate content (SO <sub>3</sub> )	2.5 ± 0.2%	< 3.0%
Chloride content	< 0.08%	≤ 0.1%
Loss of ignition (LOI)	< 3.0%	Not defined
Insoluble residue (IR)	< 3.0%	< 5.0%

## Experimental program

### Materials

#### Binding agents

An Ordinary Portland Cement (OPC) classified under CEM I 42.5N complied with EN 197-1 [32] and SLS 107 [33] was used as the primary binding agent. Table 1 represents the properties of the used OPC. As a mineral admixture, type 1—dolomitic hydrated lime conforming to ASTM C207 [34] and ICTAD SCA/4/I [35]—was also obtained for the study. Table 2 mentions the chemical compositions of the lime. The above materials were selected based on the widely usage by the local construction industries.

**Table 2** Chemical and mineralogical properties of the constituents (%)

	SiO <sub>2</sub>	Al <sub>2</sub> O <sub>3</sub>	Fe <sub>2</sub> O <sub>3</sub>	CaO	MgO	SO <sub>3</sub>	Na <sub>2</sub> O	K <sub>2</sub> O	CO <sub>2</sub>
<i>Chemical properties</i>									
Hydrated lime	0.35	0.13	0.07	88.91	4.32	–	–	–	2.01
RS	97.53	2.84	0.19	0.00	0.00	0.00	0.00	0.76	–
MS (HG)	73.59	7.59	4.83	3.07	1.02	0.00	1.75	1.33	–
MS (CH)	72.01	7.83	2.09	3.95	0.25	0.00	2.08	2.54	–
OS	65.84	15.24	4.78	2.55	2.09	0.00	0.00	0.00	–
	Calcite	Quartz	Albite	K-Feldspar	Anorthite	Dolomite	Illite	Biotite	
<i>Mineralogical properties</i>									
MS (HG)	0.62	49.48	10.44	10.68	20.30	0.22	6.23	0.02	
MS (CH)	18.97	27.95	18.03	27.15	4.36	0.23	1.66	0.00	

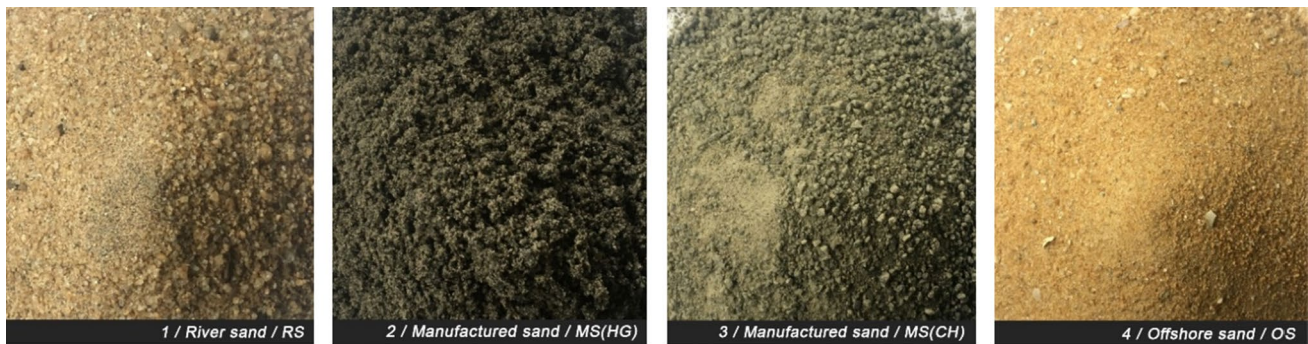


**Fig. 1** Selected fine aggregates for the study

understanding is mandatory on the performance of masonry and brick–mortar bond made with river sand alternatives in order to check the efficacy of such alternatives in the masonry field.

#### Fine aggregates

Four different types of fine aggregates as shown in Fig. 1 were selected for casting the mortars with varying mix proportions. River sand (RS) was used to produce the control mortars which were considered as the base to compare the

mortars with alternatives. Manufactured sand (MS) and off-shore sand (OS) were utilized for completely replacing the RS. Two types of MS were selected based on the parent rocks used for the manufacturing: MS from Hornblende-Gneiss rock—MS (HG)—and MS from Charnockite rock—MS (CH). Table 2 also displays the chemical and mineralogical properties of used fine aggregates. It is delighted to see that no potentially detrimental minerals for the cement-based mixes were detected in the above rocks which are stated in ASTM C294 [37]. OS was directly extracted from an open stock pile with the reduced chloride content of 0.086%, the salt level of 0.016% and the shell content of 7.45%.

Table 3 includes some of the physical properties of the used fine aggregates. All of the mentioned physical properties were investigated in the laboratory, and the standards referred for each experiment are also listed. The microfine content in fine aggregates may significantly influence both fresh and durability properties of mortar, which should be controlled [38]. MS (HG) and MS (CH) revealed higher amounts of microfines (i.e., in the range of 3–7%) than RS

and OS (0.18% and 0.24%, respectively). BS 882 [39] set a limitation on the allowable microfine content in MS as 16%. When comparing this tolerable limit, the selected MS types were complied with the standard, hence no actions were carried out to control the microfine content. There are no restraints available in the standards concerning the maximum shell and salt contents in OS. Therefore, the selected OS was directly used to prepare the mortars.

The chloride content in OS may also affect the durability of mortars. The OS selected for this study was collected after an exposure to a considerable period of washing. This reduced the chloride content to an acceptable range of 0.086%. The allowable limitations on chloride content can be found from the standards BS 5328 [40] and BS EN 998-2 [41]. BS 5328 [40] defines the maximum allowable chloride level in OS as 0.1–0.4% when it is used as the main fine aggregate in special and pre-stressed concretes. BS EN 998-2 [41] states a limit of 0.1% by the mass of fine aggregate for using in concrete and mortar. Moreover, Dias et al. [42] have already implemented some experiments using the

**Table 3** Physical properties of fine aggregates

Property	RS	MS (HG)	MS (CH)	OS	Standard
Fineness modulus	3.113	3.107	3.086	2.128	ASTM C144 [36]
Specific gravity	2.64	2.71	2.70	2.67	ASTM C128 [43]
Fine content <0.075 mm (%)	0.18	6.28	3.37	0.24	ASTM C117 [44]
Void content (%)	38.143	38.942	39.167	38.256	ASTM C29 [45]
Loose density (kg/m <sup>3</sup> )	1643.15	1783.94	1739.93	1580.32	ASTM C1252 [46]
Water absorption (%)	0.95	1.2	1.1	0.75	ASTM C70 [47]
Surface moisture (%)	1.675	4.968	2.371	2.427	ASTM C70 [47]
Clay and friable content (%)	1.59	0.77	0.39	1.18	ASTM C142 [48]
Silt content (%)	0.29	2.88	1.92	0.95	
Chloride content (%)*	–	–	–	0.086	
Salt content (%)*	0.0039	–	–	0.016	
Shell content (%)*	–	–	–	7.45	

\*Provided by the supplier

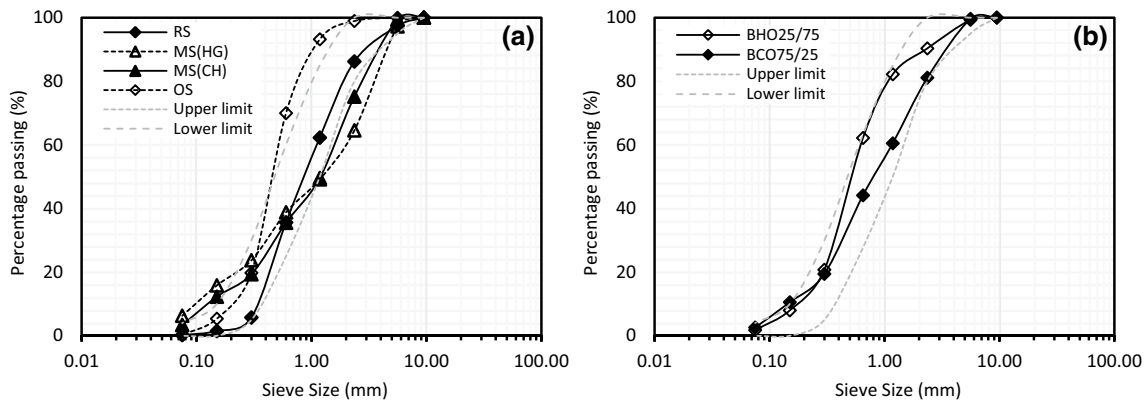


**Fig. 2** Gradation curves of fine aggregates complying with ASTM C144 [36]: **a** main sand types and **b** blended sands types

OS collected from same stockpile selected for this study and concluded the risk-free usage of OS in concrete.

Figure 2 illustrates the gradation curves of the fine aggregates. Based on Fig. 2a, RS lied within the gradation range provided by ASTM C144 [36]. However, MS and OS did not comply with the requirements for some particle size ranges. Therefore, the blending concept was introduced in this study to overcome the problems raised on the particle size distribution of the alternatives. Figure 2b represents the gradation curves after the blending of MS and OS at the pre-defined ratios. As observed, the above problems were solved to an extent, where it can be proved that the passing percentages complied the required limits.

This study deals with the mechanical properties of masonry and brick–mortar joint with varying fine aggregate contents and replacements. Characteristics of fine aggregates may act a vital role on the strength of masonry and brick–mortar bond. Angularity index ( $f_A$ ), surface roughness index ( $f_i$ ) and particle packing density ( $\rho$ ) of the selected fine aggregates were evaluated at the early stage of this study when they were in natural and blended forms. The angularity index of fine aggregates basically determines the shape of the particle whether round or cubical. A quantitative method suggested by Murdock [49] was used to estimate the angularity index of each fine aggregate. Furthermore, the standard testing method provided in ASTM D3398 [50] was referred to analyze the surface roughness index of fine aggregates.

Figure 3a shows the angularity and surface roughness indexes of the fine aggregates incorporated in the mortars used to fabricate the specimens. It can be identified that both indexes were increased as BHO25/75 < RS100 < BCO75/25 < MH100 < MC100. Among the selected fine aggregates, RS and OS are naturally available and processed through years of attrition. This enables the particles more rounded with smoother surface texture. MS is purposely made crushed fine product which enables more cubical particles and rougher

surface texture. This trend can be clearly observed from the increased indexes of MH100 and MC100 than RS100 and the blended sand types such as BHO25/75 and BCO75/25.

A rodding procedure was followed up according to ASTM C29 [45] to evaluate the packing density of fine aggregates. Various gradation curves may influence the packing density of fine aggregates and the density of mortars. When MS and OS are in natural form, some parts of the gradation curves did not comply with the requirements, while RS substantially lied within the allowable region. However, the increased packing density of MS can be due to the higher presence of microfine which has the ability of micro-filling effect. This problem was resolved when MS was replaced with OS, which showed greater packing densities of BHO25/75 and BCO75/25 as represented in Fig. 3b. Therefore, it was identified that both microfine content and uniform gradation significantly increased the packing density of fine aggregates.

### Solid clay bricks

Clay bricks are typically manufactured from manual molding processes and burnt in kilns in Sri Lanka. The solid clay bricks which are locally available and conventionally used were utilized as the walling unit for this study. Standard procedures provided in ASTM C67 [51] were followed for analyzing the compressive strength, flexural strength, water absorption and initial water absorption (IRA) of the selected bricks. The compressive and flexural strength determinations were carried out using a Universal Testing Machine with an accuracy of 0.1 N. Table 4 summarizes the average values of the properties of the clay bricks.

All the required bricks were collected from a single supplier throughout the study in order to ensure the uniqueness of the materials used for brick production, manufacturing process and workmanship. After utilizing, the bricks were stored in a room temperature of  $30 \pm 2$  °C in order to avoid any dimensional changes and other related factors.

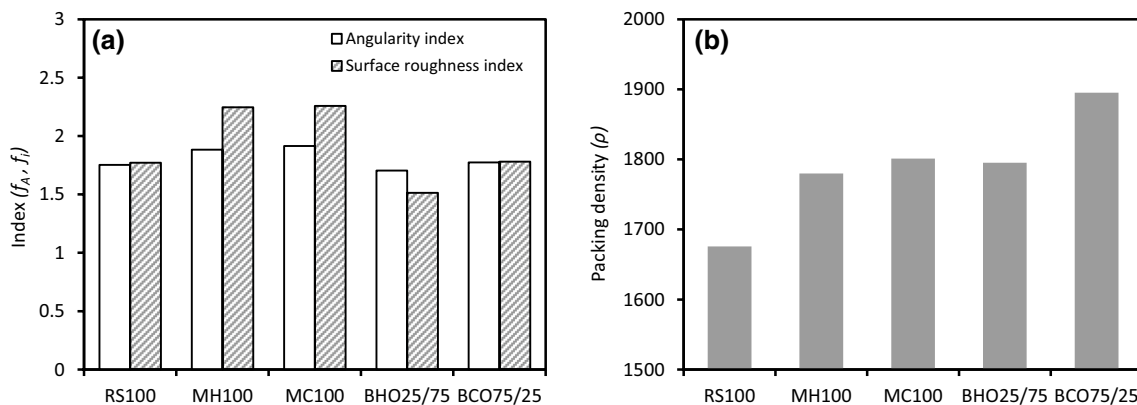


Fig. 3 Particle indexes and packing density of fine aggregates contained in the mortars



The coefficient of variation was evaluated to check the effects of the properties of bricks on the performance of masonry and brick–mortar joint. Regarding the mechanical properties of bricks, the compressive strength test results showed an average coefficient of variation in individual samples as 2.169% and the flexural strength test results proved an average coefficient of variation in individual specimens as 1.055%. No significant variation in the compressive strength and flexural strength was observed between the brick samples. Hence, it was discerned that the variation in strength parameters of the bricks did not significantly affect the characteristics of masonry and brick–mortar joint.

Similarly, the other properties of brick also revealed a small coefficient of variation in the individual specimens. The coefficient of variation in water absorption and initial rate of absorption were 0.89% and 1.84%, respectively. Hence, these properties also did not significantly affect the characteristics of masonry and brick–mortar joint. Due to the small contribution of the characteristics of solid clay bricks, it can be deduced that the variation in the mechanical properties of masonry and brick–mortar joint were mainly controlled by the mortars comprised of different fine aggregate contents.

**Table 4** Properties of solid clay bricks

Property (No of samples tested)	Average value
Dimensions $L \times W \times H$ , mm <sup>3</sup> (10)	190 × 95 × 50
Unit weight, kg/m <sup>3</sup> (10)	1551.911 (0.51)
Compressive strength, MPa (20)	4.165 (2.17)
Flexural strength, MPa (10)	0.698 (1.06)
Water absorption, % (10)	19.856 (0.89)
Initial rate of absorption, kg/m <sup>2</sup> /min	9.647 (1.84)

Values in parenthesis represent the coefficient of variation in the result, %

**Table 5** Mix design of mortars, kg/m<sup>3</sup>

Mortar type	Designation	Lime	Cement	Fine aggregate				Water
				RS	MS(HG)	MS(CH)	OS	
CM	CM/RS100	–	450	2258 (100)	–	–	–	225
	CM/MH100	–	450	–	2318 (100)	–	–	225
	CM/MC100	–	450	–	–	2310 (100)	–	225
	CM/BHO25/75	–	450	–	580 (25)	–	1713 (75)	225
	CM/BCO75/25	–	450	–	–	1732 (75)	571 (25)	225
LCM	LCM/RS100	186	525	1976 (100)	–	–	–	263
	LCM/MH100	186	525	–	2028 (100)	–	–	263
	LCM/MC100	186	525	–	–	2021 (100)	–	263
	LCM/BHO25/75	186	525	–	507 (25)	–	1499 (75)	263
	LCM/BCO75/25	186	525	–	–	1516 (75)	500 (25)	263

Values in parenthesis are the contribution of fine aggregate, %

## Mortars and mix design

The two main types of mortar were cast: 1:6 cement–sand (CM) mortars and 0.5:1:4.5 lime–cement–sand (LCM) mortars. These ratios are commonly used for various masonry appliances by the local construction industries. ASTM C270 [52] also briefly describes the practical applications of the above mixing proportions. Table 5 tabulates the mix design of each mortar according to the weight-basis. Initially all the mix designs were carried out with a w/c of 0.5. However, in order to maintain the workability throughout the experiment, the flow of mortar was regularly measured according to EN 1015-3 [53] until it reached a flow of  $110 \pm 5$  mm.

Table 6 shows the average mechanical properties of mortars at the effective w/c ratios ( $w/c_e$ ). Required specimens for the mortar tests were prepared during the fabrication of masonry specimens. When contemplating the water requirements to achieve the defined flow, mortars with RS alone revealed a lower water demand than the mortars contained MS (HG). Mortars with MS (CH) proved a slightly lower water requirement than the RS mortar. The total specific surface of MS is usually increased as a result of higher microfine levels. This may significantly increase the water requirement for mortar to achieve the required flow. A considerable water demand was also observed with the mortars contained 25% and 75% of OS.

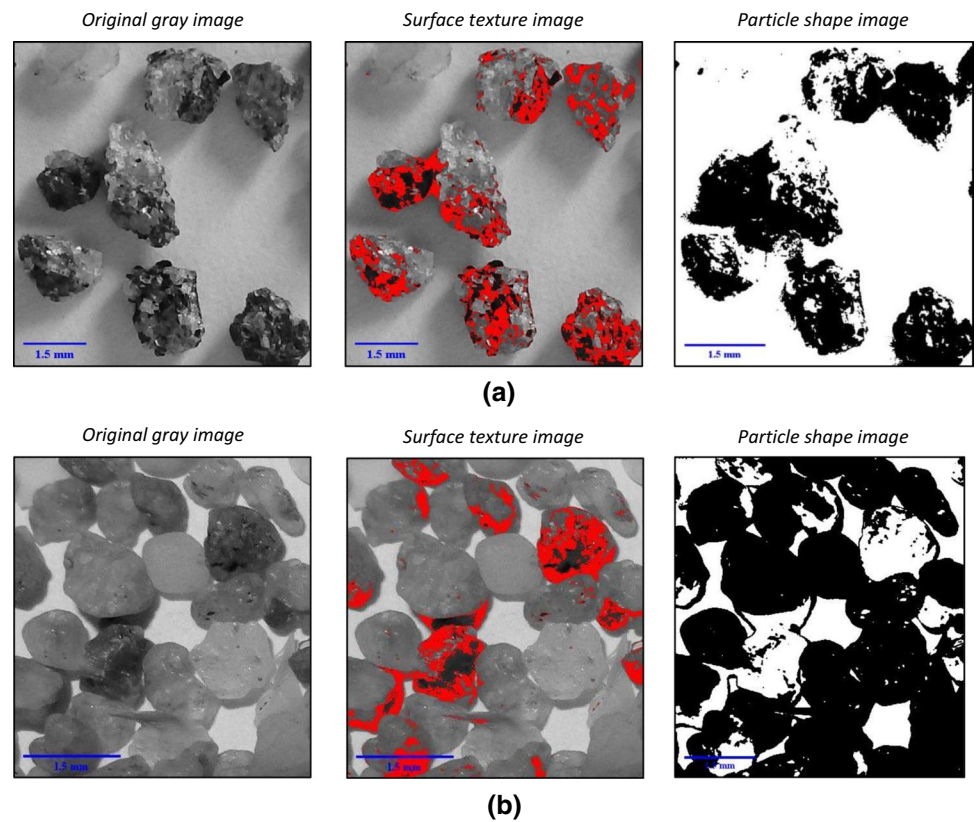
The compressive strength and flexural strength of mortars were determined at 28 days from the casting as per EN 1015-11 [54], and the linear shrinkage was investigated after 7 days based on ASTM C531 [55]. Higher compressive and flexural strengths were noticed with the MS mortars. Mortars with blended fine aggregates also showed improved strengths than the RS mortars. Here, the particle physical characteristics such as shape and surface texture mainly influenced the mechanical properties of mortar. It is obvious that the mechanical properties of mortars directly depend on the interactions between the cement paste and aggregates. In

**Table 6** Average mechanical properties of mortars

Designation	w/c <sub>i</sub>	w/c <sub>e</sub>	Compressive strength, $f_{cm}$ (MPa)	Flexural strength, $f_{lm}$ (MPa)	Linear shrinkage, mm
CM/RS100	0.5	0.76	17.5 (5.2)	2.1 (11.2)	0.011 (2.1)
CM/MH100	0.5	0.81	21.3 (6.8)	2.6 (8.4)	0.023 (5.1)
CM/MC100	0.5	0.68	29.4 (4.1)	4.5 (7.9)	0.034 (3.8)
CM/BHO25/75	0.5	0.78	13.4 (3.7)	1.9 (4.7)	0.026 (4.7)
CM/BCO75/25	0.5	0.71	19.5 (9.4)	2.5 (2.7)	0.029 (6.5)
LCM/RS100	0.5	0.53	28.6 (4.1)	4.5 (6.1)	0.006 (12.6)
LCM/MH100	0.5	0.64	36.7 (6.3)	5.2 (6.7)	0.017 (10.7)
LCM/MC100	0.5	0.53	37.5 (3.1)	5.6 (5.4)	0.019 (4.7)
LCM/BHO25/75	0.5	0.57	31.2 (3.7)	4.4 (9.7)	0.008 (8.9)
LCM/BCO75/25	0.5	0.52	35.4 (8.7)	4.7 (4.3)	0.011 (5.1)

Values in parenthesis represent the coefficient of variation, %

**Fig. 4** Processed micro-images of particles in the range of 1.4–2.8 mm: **a** MS particles and **b** OS particles



this study, the cement type was maintained constant for each mortar. Therefore, the mechanical performance of mortars or the properties of cement paste–aggregate interface can be directly related to the characteristics of fine aggregates.

Figure 4 represents the processed images of MS and OS particles in the range of 1.4–2.8 mm using an image processing software. The first image of each sand type shows the gray scale of original digital microimage of the particles. To study the influence of surface texture characteristics, the grayscale images were further processed to obtain the threshold images (at 10% peak intensity). In the

corresponding images, the red shades, black shades and gray shades indicate different phases of the surfaces. Here, the greater number of shades in the surfaces defines the more roughness of the particles. Furthermore, b/w images were obtained from the original gray images to visually analyze the angularity of particles. The b/w images were then converted into threshold images (at 20.5% peak intensity) to identify the shape characteristics.

Regarding the surface properties, MS particles revealed more color shades comparing with OS particles. It can be clearly observed that each MS particle contained more than

a single-color shade which defines different phases of particle surface. However, most of the OS particles manifested a single-color shade (gray shade) which concludes the more smoothness of surfaces (i.e., surface with one phase) than the MS particles. When concerning the shape characteristics, it can be distinctly identified that the MS particles were more angular (i.e., having sharp edges) than the OS particles with round edges.

The CM and LCM mortars with MS alone showed higher compressive and flexural strengths than the RS mortars and blended sand mortars. This could be due to high bonding characteristics between the particles and cement paste due to the high surface roughness and angularity. These properties could improve the interlocking between the particles and cement paste during the hardening stages of mortars. Considering the mechanical properties of CM and LCM mortars incorporated the blending of MS and OS, the compressive and flexural strengths were considerably reduced than the MS mortars. In blended sands, the MS particles were resembled with smooth and rounded OS particles which declined the resultant angular and rough particles in the mortars. Hence, the bonding characteristics between cement paste and blended sand particles could be reduced as a result of the poor interconnection between the constituents.

Moreover, different constituents of fine aggregate could also affect the properties of mortar. Figure 5 shows the typical surface characteristics of mortars with the selected alternatives. This investigation was carried out in order to identify the total specific surface area of mortars. All mortar specimens manifested pores with different scales in the surfaces. Here, the macropores are defined in the range of

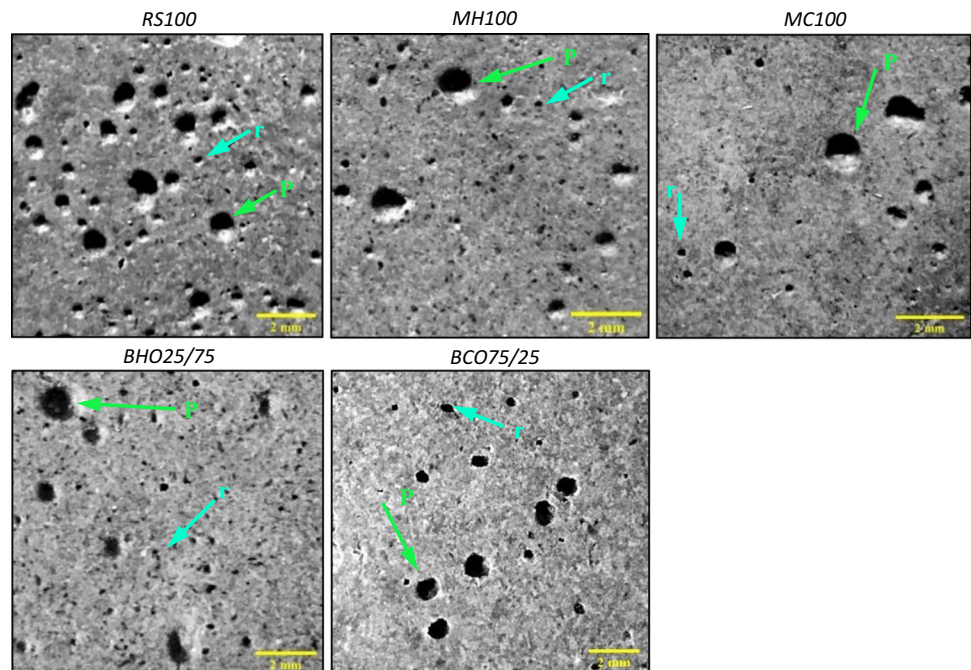
1–1.5 mm and the micropores are less than 1 mm. RS100 mortar revealed considerably higher macro pores than other mortars. Concerning the mortars with MS alone such as MH100 and MC100, the presence of macro- and micropores was reduced due to the considerable microfine aggregates in MS than RS. From these visual inspections, it can be concluded that the microfine aggregates significantly increased the total specific surface of mortars.

Comparing with MS mortars, the blended sand mortars showed higher presence of macro pores which was due to the replacement of MS with OS. However, the total specific surface of BHO25/75 and BCO75/25 mortars was larger than the RS100 mortar as a result of the lower fineness modulus of OS particles. From the microimages of BCO75/25 mortar, it can be distinctly observed that a very few micropores were presented comparing with the other mortars. In this case, the presence of microfines in MS and the inclusion of tiny OS particles significantly increased the total specific surface. These observations can be numerically compared with the results provided in Fig. 3b.

### Specimen preparation and test methods

The experiments were conducted to investigate the performance of masonry and brick–mortar joint which were fabricated using the defined mortars. The following specimens were prepared for the masonry tests: compressive strength test—stack bond prisms, diagonal tensile strength test—running bond walls and flexural strength test—stack bond prisms. For investigating the shear strength and adhesive strength of

**Fig. 5** Surface morphology of a typical mortar type with different sand inclusions ( $P$ —macro pore;  $r$ —micropore)





brick–mortar bonds, the triplet samples and cross-couplet samples were prepared, respectively.

For each experiment, bricks were immersed in water for 24 h prior to the specimen casting. During the laying, bricks were ensured with no moisture present on the surfaces. Several studies proved that the strength of masonry directly depends on the surface moisture of bricks [56, 57]. The mortar thickness was maintained in both horizontal and vertical joints as  $12 \pm 2$  mm. All the specimens were covered with moist polyethylene bags and kept in a cabinet with a room temperature of  $30 \pm 2$  °C for 28 days. During the first 20 days of curing, the specimens were uncovered once a day and thoroughly sprayed with water.

### Compressive strength of masonry

The compressive strength is considered as one the primary properties of masonry. The study by Haach et al. [58] proved that the mortar has a slight effect on the compressive strength of masonry. Here also the influence of the compressive strength of mortars on the compressive strength of masonry was evaluated. Five brick units were bonded in stretcher position with four mortar joints to prepare the specimens as shown in Table 7a (with  $h_p/t_p = 3.36$ , where ASTM C1314 [59] suggests a range of 1.3–5.0 for prism compression tests). Three test samples were cast for each mortar to determine the average compressive strength of masonry as specified by ASTM C1314 [59]. During the testing, prisms were capped with 15-mm-thick steel bearing plates at the top and bottom to ensure a uniform stress throughout the area of specimen. The compressive strength of masonry ( $f'_m$ ) was determined as the ratio between peak compressive load ( $P$ ) sustained and the net cross-sectional area of specimen ( $A_n$ ) as given in Eq. (1).

$$f'_m = P/A_n \tag{1}$$

### Diagonal tensile/shear strength of masonry

The diagonal tensile strength was tested on the running wall specimens according to the loading setup displayed in Table 7b. Solid steel shoes were placed along the diagonal axis of the specimen at 875 mm (diagonal length of wall), and the compression load was applied vertically downwards to the top shoe. The load applied on the specimens acted as combined diagonal tension and shear stress. While fabricating the wall specimens, the work size of a unit (brick + mortar) with both horizontal and vertical joints was ensured as  $202 \times 107 \times 62$  mm<sup>3</sup>. Complying with ASTM E519 [60], three half-brick running bond walls were prepared with each mortar for the determination of shear stress ( $S_s$ ) with respect

to maximum applied load ( $P$ ) and the net area of specimen ( $A_n$ ) according to Eq. (2).

$$S_s = 0.707 \times P/A_n \tag{2}$$

Here,

$$A_n = (w + h)tn/2$$

where w: width of the specimen, h: height of the specimen, t: total thickness of the specimen, n: percentage of the gross area of solid units.

### Flexural strength of masonry

Flexural strength test was executed perpendicular and parallel to the bed joints on the masonry assemblages as shown in Table 7c. As provided in ASTM E518 [61], a third-point loading method and a uniform loading method were followed for the loading parallel and perpendicular to the bed joints, respectively. The supports were positioned at a span length ( $l$ ) of 350 mm to sustain the weight of prism. Three stack bonded prisms were made for each mortar using six bricks affixed in stretcher position with five mortar joints. Equation (3a) and (3b) was used for identifying the modulus of rupture under third-point loading ( $R_t$ ) and uniform loading ( $R_u$ ), respectively. Here,  $P$ : peak flexure load,  $P_s$ : weight of specimen,  $b$ : average width of specimen and  $d$ : average depth of specimen.

$$R_t = (P + 0.75P_s)l/bd^2 \tag{3a}$$

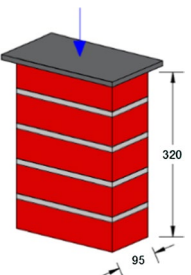
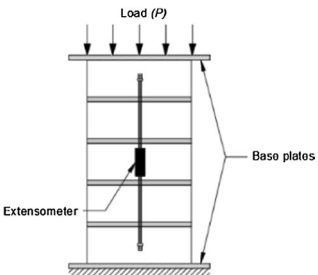
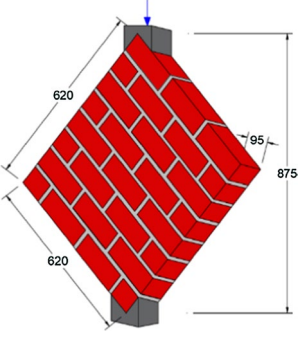
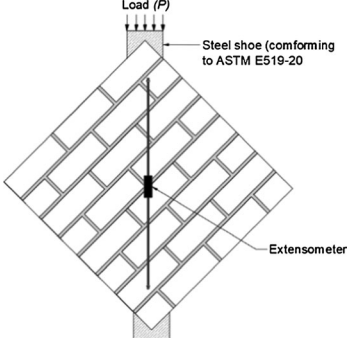
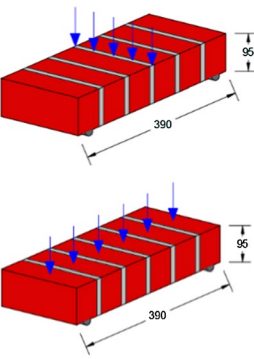
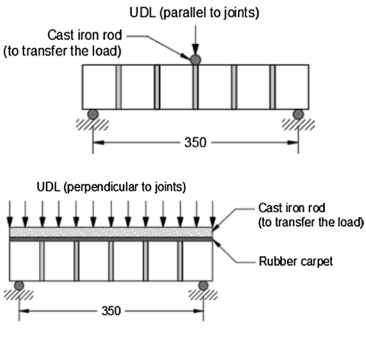
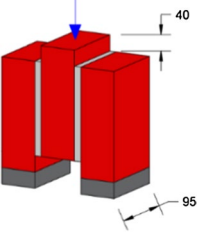
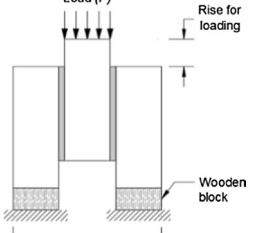
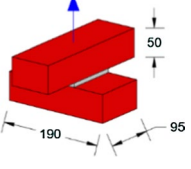
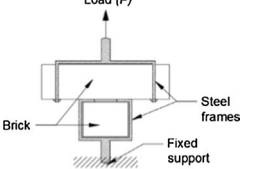
$$R_u = 0.75(P + P_s)l/bd^2 \tag{3b}$$

### Shear strength of brick–mortar bond

A typical triplet specimen as exhibited in Table 7d was used for analyzing the shear strength of brick–mortar bond. In order to allow a vertical movement of the middle brick, a 40 mm rise was provided to apply the load (reduced brick–mortar contact area of  $150 \times 95$  mm<sup>2</sup>), while the movements of adjacent bricks were restrained on wooden blocks. Three triplet specimens were fabricated for each mortar. The shear bond strength ( $\tau_s$ ) was calculated using Eq. (4), concerning the maximum shear load ( $P$ ) resisted, area of the left side joint ( $A_1$ ) and area of the right side joint ( $A_2$ ) as suggested by RILEM TC 127-MS-B.4 [62].

$$\tau_s = P/(A_1 + A_2) \tag{4}$$

**Table 7** Masonry specimen types and loading arrangements (all dimensions are in mm)

Experiment	Type	Specimen diagram	Loading arrangement
(a) Compressive strength	Stack bonded prism		
(b) Diagonal tensile/shear strength	Running wall		
(c) Flexural Strength	Stack bonded prism		
(d) Shear bond strength	Triplet		
(e) Adhesive bond strength	Couplet		

**Adhesive strength of brick–mortar bond**

A direct tension load was applied on the cross-couplet specimens as illustrated in Table 7e to investigate the adhesive

strength of brick–mortar bond. Three cross-couplet specimens were cast based on the provisions given in ASTM C952 [63] for each mortar. During the test, the lower brick was kept inside a steel frame which was fixed to a support.

The upper brick was also kept inside a similar steel frame and the direct tension load was applied to it. For each couplet specimen, a contact area ( $A_j$ ) of brick and mortar was maintained as  $95 \times 95 \text{ mm}^2$  with the mortar thickness of 12 mm. The adhesive bond strength ( $\delta_A$ ) was determined based on Eq. (5), when a cross-couplet specimen failed at a tension load ( $P$ ) with brick–mortar joint area of  $A_j$ .

$$\delta_A = P/A_j \tag{5}$$

## Results and discussion

The influence of RS alternatives and the replacement levels on the properties of masonry and brick–mortar joint, the stress–strain relationships and the most common failure types observed during each experiment. Each value mentioned in Table 8 represents the average result after 28 days of curing of masonry specimens. The results on mechanical properties of masonry such as compressive strength ( $f'_m$ ), diagonal tensile/shear strength ( $S_s$ ), modulus of rupture parallel to mortar joints ( $R_t$ ) and modulus of rupture perpendicular to mortar joints ( $R_u$ ) are listed. Furthermore, the mechanical characteristics of brick–mortar bond such as shear bond strength ( $\tau_s$ ) and adhesive strength ( $\delta_A$ ) are also included.

### Compressive stress–strain relationships, failure investigation and influencing parameters

The mean compressive strength of masonry provided in Table 8a proves that, when CM and LCM mortars incorporated MS alone, the compressive strength of masonry was slightly increased than the specimens made with control mortars (RS100). It was observed that the CM mortars such as MH100 and MC100, respectively, revealed around 6% and 2% more compressive strength than the RS100 mortar. When considering the prisms with blended sand CM

mortar, BHO25/75 manifested a slightly lower compressive strength than the masonry with reference mortar. However, BCO75/25 showed a considerably higher strength than RS100 masonry.

Regarding the LCM mortars, masonry comprised of each mortar with the selected RS alternatives and the replacement levels increased the compressive strength than the reference mortar masonry. Figure 6a illustrates the stress–strain relationships of the masonry prisms constructed with the selected mortar types under compression. A bilinear behavior can be noticed with each masonry up to the optimum compressive stress. At the initial compression stages, masonry prisms revealed a large displacement with respect to the applied stress which was due to the crushing of bricks. After that the masonry prisms showed gradually increasing linear relationships. The prisms with LCM mortars attained the maximum compressive stress at lower strain levels than the prisms with CM mortars. This justifies the higher compressive strength of CM mortars over the LCM mortars.

Several studies proved that the relationship between the compressive strength of masonry and the compressive strength of mortar was used to prepare the masonry [2, 19]. From the relevant studies, all authors provided a powered relationship between the above properties in a common format. Similarly, here also an investigation was made on this concept, where Fig. 7 exhibits the relationship between the above properties based on the average compressive strengths obtained. A nonlinear relationship as provided in Eq. (6) can be obtained with an acceptable coefficient of determination, R-squared of 0.7874.

$$f'_m = 0.57(f_{cm})^{0.41} \tag{6}$$

It should be also noticed that the cement content was maintained constant for each CM and LCM mortar. Therefore, the compressive strength of masonry can be directly related to the physical characteristics of fine aggregate included in the mortars as discussed in the previous sections. Sand particle

**Table 8** Summary of the results of masonry and brick–mortar bond tests

Designation	a $f'_m$ (MPa)	b $S_s$ (MPa)	c $R_t$ (MPa)	d $R_u$ (MPa)	e $\tau_s$ (MPa)	f $\delta_A$ (MPa)
CM/RS100	2.343	0.184	0.073	0.082	0.527	0.064
CM/MH100	2.485	0.211	0.096	0.123	0.702	0.075
CM/MC100	2.394	0.161	0.104	0.131	0.729	0.069
CM/BHO25/75	2.336	0.230	0.074	0.086	0.597	0.074
CM/BCO75/25	2.587	0.196	0.091	0.103	0.660	0.079
LCM/RS100	1.748	0.254	0.100	0.270	0.232	0.057
LCM/MH100	2.215	0.295	0.112	0.284	0.263	0.059
LCM/MC100	2.172	0.284	0.121	0.275	0.281	0.063
LCM/BHO25/75	1.842	0.201	0.097	0.216	0.230	0.067
LCM/BCO75/25	1.861	0.154	0.112	0.276	0.274	0.073

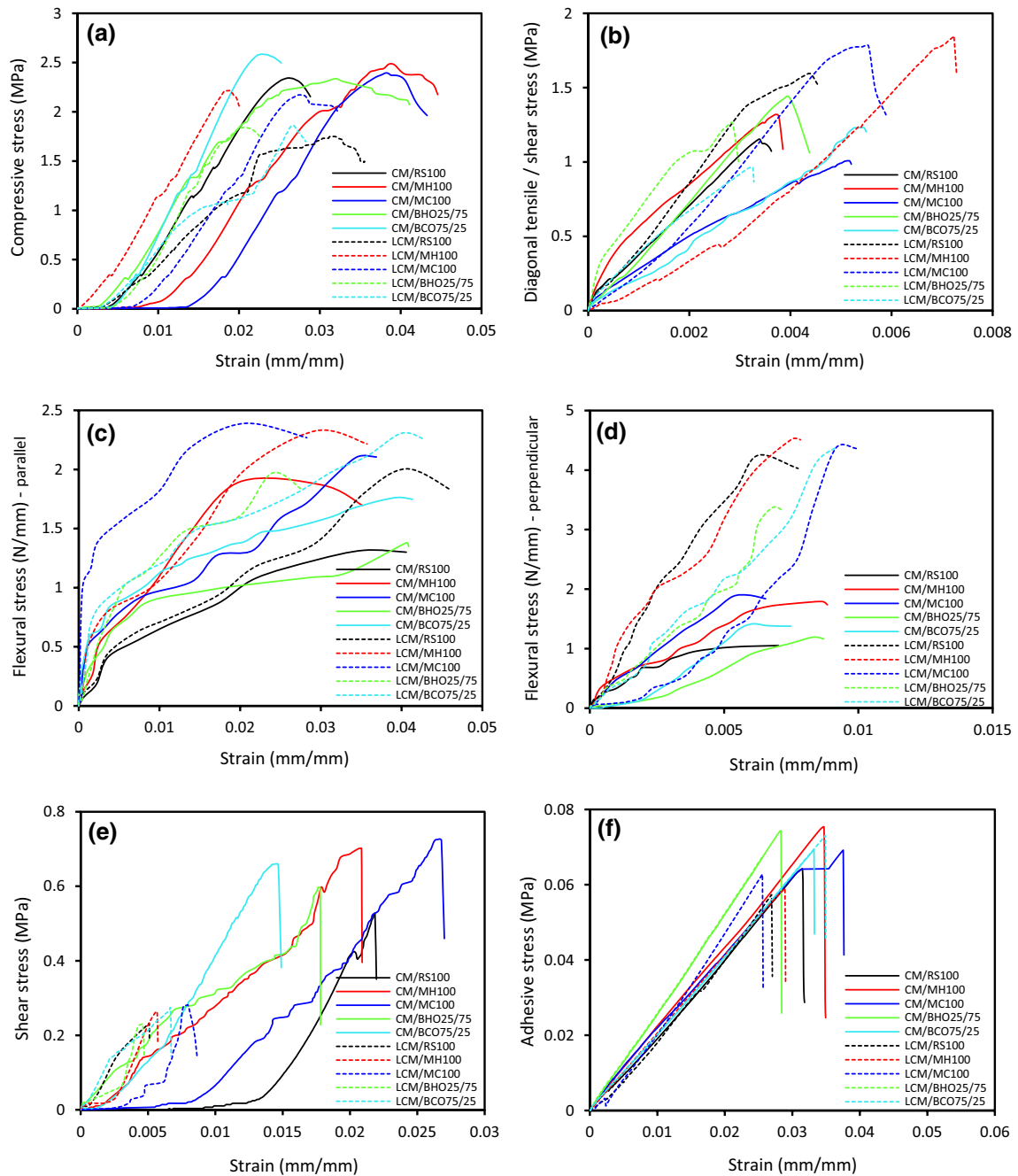


**Fig. 6** Shear stress–strain curves of masonry prisms and brick–mortar joints under different loading cases

characteristics such as angularity and surface roughness are the determining parameters of the compressive strength of mortar [38]. The dependence of compressive strength of mortars and masonry prisms on the particle characteristics can be clearly understood where MH100 and MC100 mortars revealed the highest compressive strengths due to a well interlocking and the slipping resistance of MS particles. These compressive strengths were reduced to an extent when MS was partially replaced by OS in the mortars. Therefore,

from a multiple regression analysis at 95% confidence interval, the compressive strength of masonry can be correlated with the compressive strength of mortar, the angularity index ( $f_A$ ) and the surface roughness ( $f_i$ ) of fine aggregates with an adjusted R-squared value of 0.6994 as provided in Eq. (7).

$$f'_m = -0.0005f_{cm} + 0.3f_A - 0.08f_i - 0.31 \tag{7}$$



Investigation on identifying the failure patterns of masonry prisms under the compression was initiated after specimens reached the maximum stress. The failure types of masonry under compression were classified from the length and shape of cracks propagated in the front and side surfaces of the specimens and the locations of cracks based on ASTM C1314 [59]. These observations were made on each tested sample during the experiment; however, Fig. 8 represents the most common failure types observed during the experiment such as face shell separation, shear break and tension break. From the observations, there was no relationship between the failure behavior and the mortar of the masonry observed.

### Diagonal tensile/shear stress–strain relationships and failure investigation

The shear strength of masonry was evaluated using the half-scale masonry wallets subjected to a uniform compression stress. Three specimens were prepared for each mortar, and the average results are listed in Table 8b. Similar to the results obtained with the compressive strength test of

masonry, increased shear strength/diagonal tensile strengths were observed when mortars included MS alone. Masonry with CM/MH100 mortar resulted 15% higher shear strength than CM/RS100 masonry. Masonry made with blended sand mortars such as CM/BHO25/75 and CM/BCO75/25 also revealed improved performances (i.e., around 25% and 7% higher, respectively) than the CM/RS100 masonry.

Considering the masonry with LCM mortars, MH100 and MC100 mortars showed considerably greater shear strengths than the RS100. However, the blended sand mortars declined the shear strength of masonry than RS100. Hence, the shear strength of masonry was reduced as MH100 > MC100 > RS100 > BHO25/75 > BCO75/25. According to Fig. 6b, the stress–strain relationship of masonry wallets manifested a linear gradual increase from the point of load applied up to the maximum shear stress achieved.

An attempt was initially done to determine the relationship between shear strength of masonry and the shear strength of brick–mortar bond. The masonry wallets were subjected to a compressive stress which was then transformed to a shear stress along the brick–mortar joint. The study executed by Dehghan et al. [19] proved a powered relationship between the shear strength of masonry and the compressive strength of mortar. However, no significant interrelation between the above properties was observed in the present study.

Masonry wallets were failed with varying cracks and the splitting of specimens. Figure 9 represents the failure modes observed during the diagonal tensile/shear strength test of masonry. The failure designations were assigned as the authors' wish based on the crack patterns and their locations noticed when the masonry wallets achieved the optimum stress. As observed, a few samples revealed minor cracking behavior along the diagonal axis and out of the diagonal axis. A few more samples manifested splitting failures such as multiple splitting (i.e., specimen was fractured at different locations irrespective to the axis of failure) and two-half splitting (i.e., separation of specimen into two approximately equal portions). Most of the samples showed the combined

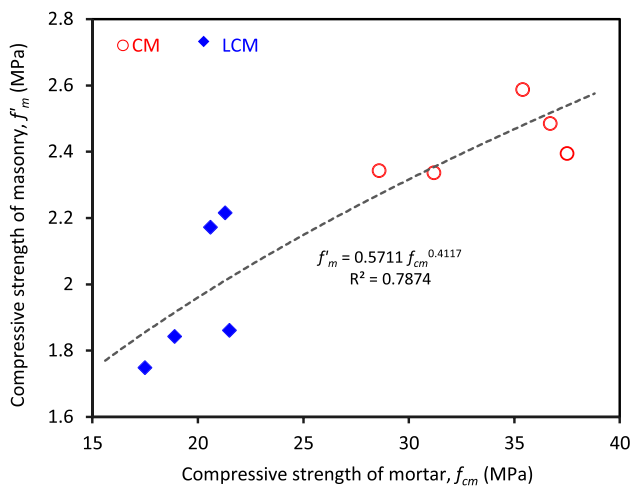


Fig. 7 Effect of compressive strength of mortar on compressive strength of masonry

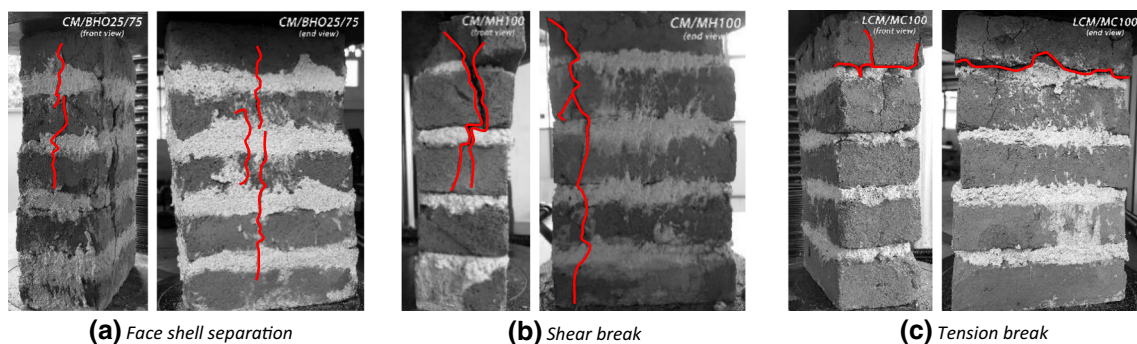
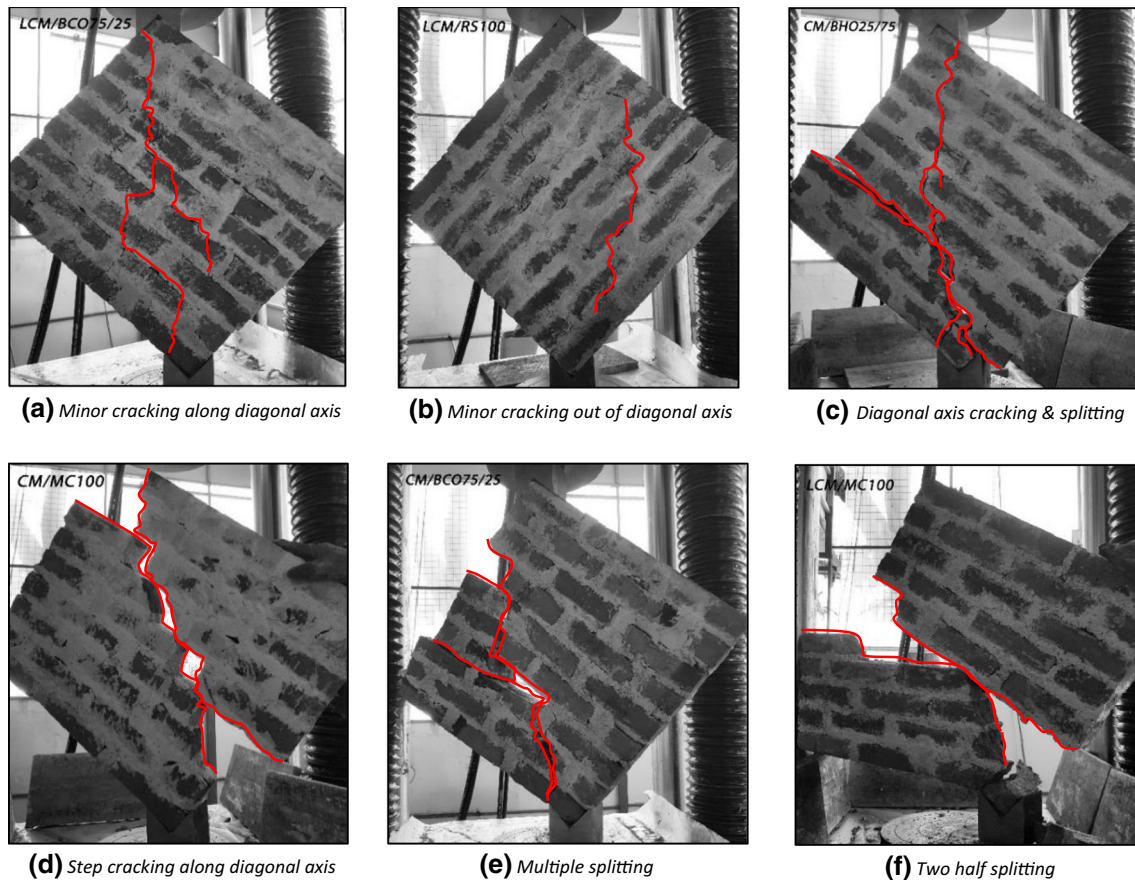


Fig. 8 Front and side views of common failure patterns under compressive stress



**Fig. 9** Failure patterns and planes of failure of masonry wallets under diagonal tensile/shear stress

diagonal axis cracking and splitting and the diagonal step cracking. Similar to the compressive strength test of masonry, here also no impacts of mortars were noticed on the failure types of masonry.

### Flexural stress–strain relationships, failure investigation and determining parameters

The strength of masonry under flexural load was investigated based on the two methods suggested by ASTM E518 [61]. The stack bonded prisms were applied with a uniform line load perpendicular (uniform loading method) and parallel (third-point loading method) to the mortar joints. For each test and mortar type, three prisms were fabricated and evaluated. The results tabulated in Table 8c, d represent the average gross area modulus of rupture determined after 28 days of curing with the stress applied parallel and perpendicular to the bed joints, respectively.

Concerning the prisms prepared with CM mortar, the modulus of rupture parallel to the bed joints was increased when MS fully replaced the RS in mortar. The masonry prisms with MH100 and MC100 mortars were come up with 32% and 42% more flexural strengths than the masonry made

with RS100. Moreover, the masonry with BHO25/75 and BCO75/25 mortars also revealed a high performance than the reference mortar masonry (i.e., 1% and 25% more than the RS100 mortar masonry, respectively). Similar trends were observed for the masonry with LCM mortars. It was noticed that, the gross area modulus of rupture parallel to the mortar joints was increased in the order of RS100 < BHO25/75 < BCO75/25 < MH100 < MC100. The gross area modulus of rupture perpendicular to the bed joints was also increased in the same order as noticed above.

From the maximum stress attained by the masonry prisms, the masonry with LCM mortars manifested higher strengths than the masonry incorporated CM mortars. This concludes that the addition of hydrated lime in mortars significantly advanced the performance against the bending of specimens which can be clearly identified from the stress–strain relationships illustrated in Fig. 6c, d. Here, non-linear relationships were noticed between the flexural stress applied parallel and perpendicular to the bed joints and the strain of masonry specimens.

When masonry prisms were placed horizontally on the supports to apply the flexural load, mortars played a vital role on bonding the solid bricks together and to keep the

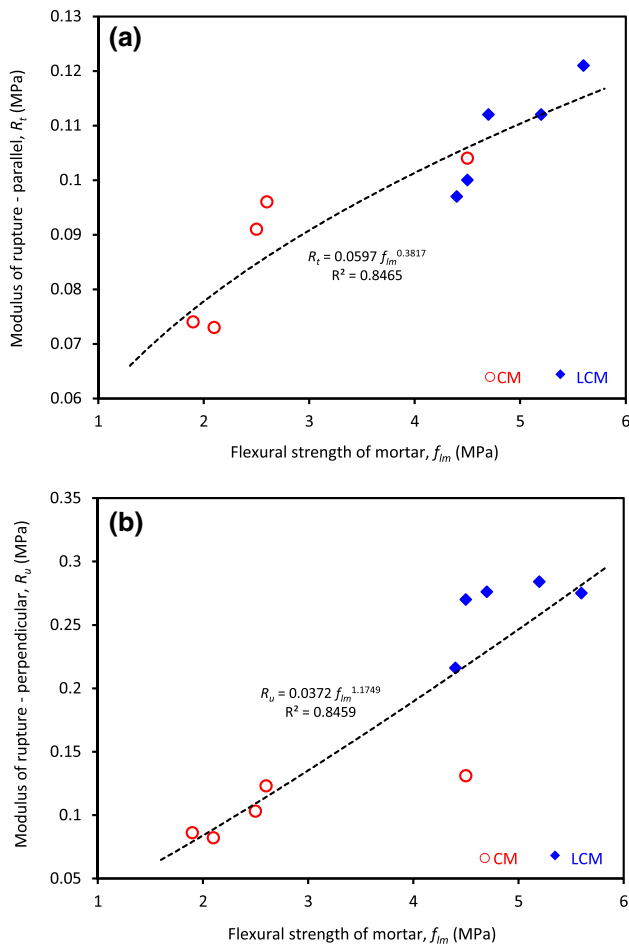


**Fig. 10** Effect of flexural strength of mortar on modulus of rupture of masonry

specimens as simply supported. Due to this, flexural strength of mortars is a primary factor which influenced the strength of masonry prisms against bending. The test results were

plotted as illustrated in Fig. 10a, b to theoretically study the effects of flexural strength of mortars ( $f_{lm}$ ) on the modulus of rupture of masonry ( $R_t$  and  $R_u$ ). The best fitting linear relationships were identified from the high R-squared values of 0.8465 and 0.8459. Equation (9a) and (9b) represents the above relationships, and thus, it can be concluded that the flexural strength of mortar is the most determining parameter for the flexural strength of masonry.

$$R_t = 0.06(f_{lm})^{0.38} \tag{9a}$$

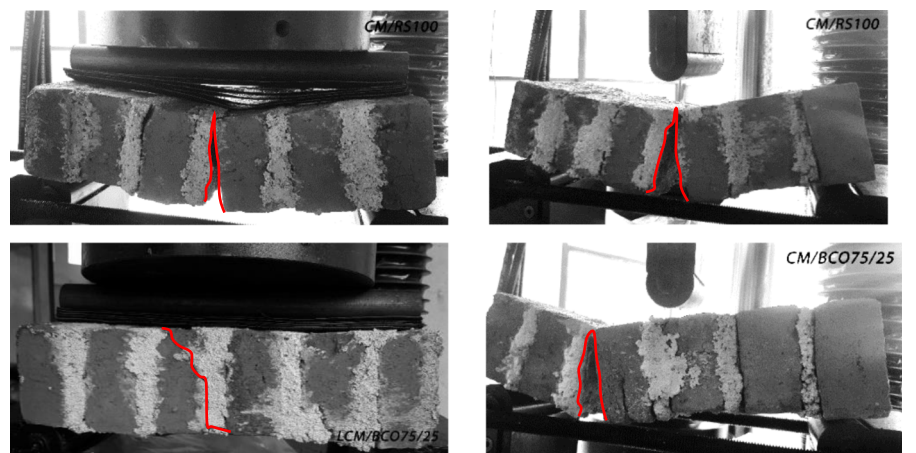
$$R_u = 0.04(f_{lm})^{1.17} \tag{9b}$$

Regarding the failure behavior of the masonry prisms under flexural stress, most of the specimens manifested a bending failure at the middle of the span. However, some prisms were failed near the supports. In most cases, the bending failure was occurred at the brick–mortar joint without any brick or mortar failure (see Fig. 11). However, a few samples were noticed with brick failure due to the low shear strength of bricks.

### Shear bond stress–strain relationships and control parameters

Shear bond characteristics of a brick–mortar junction are a salient feature in masonry constructions. Three triplet specimens were fabricated for each mortar, and the loading was performed perpendicular to the bearing surface of the middle brick which had a rise of 40 mm than the adjacent bricks. Table 8e lists the average shear strength of brick–mortar joint for each mortar type. Similar to the conclusions driven with the masonry properties, the maximum shear strength was achieved when mortar comprised of MS alone. The strengths were much deviated from the bond prepared with RS100 mortar. Regarding the joint with CM mortars,

**Fig. 11** Failure planes of masonry under flexural load perpendicular to mortar joint (a) and parallel to mortar joint (b)



**(a)** Bending failure at middle (top); shear failure of brick (bottom)

**(b)** Bending failure at middle (top); Bending failure near the support (bottom)

MH100 and MC100 revealed the best performance against the shear stress applied, which were nearly 33% and 38% more than the specimens bonded with reference mortar. The performance of triplets fabricated with blended sand mortars was also improved to an extent than the RS100 samples (i.e., around 13% and 25% more for BHO25/75 and BCO75/25, respectively).

Regarding the brick–mortar bond made with LCM mortars, RS100 mortar achieved a shear strength of 0.232 MPa which was 13% and 21% lower than the samples with MH100 and MC100 mortars, respectively. LCM mortars with the selected blended sands also manifested acceptable shear strength characteristics comparing with the reference specimen. Figure 6e shows the stress–strain relationships of the brick–mortar joints with different mortars subjected to the shear stress. Analogizing the peak values of the curves, the joints made with CM mortars are much different from the LCM mortars and this reveals that the addition of hydrated lime significantly declined the performance of brick–mortar joint against shear. Same as the compressive stress–strain curves of masonry, at the initial stage of the shear stress application triplet specimens demonstrated higher displacements which was as a result of the compression failure or the crushing of the middle brick. Each curve represented a vertical/steep decline just after the peak which was due to the sudden failure of either one or both of the joints.

Shear strength is one of the main properties of brick–mortar joint which could be affected by different fine aggregate characteristics in mortar. The particle physical characteristics such as shape index and surface texture index were also referred here to analyze such effects. As provided in Fig. 12a, acceptable correlations were noticed between the shear strength of brick–mortar joint fabricated with CM mortars and the angularity/shape index and surface roughness index. Equation (10a) and (10b) represents the linear models derived between the above properties with the R-squared values of 0.6401 and 0.5218, respectively.

$$\tau_s = 0.18(f_A)^{2.12} \tag{10a}$$

$$\tau_s = 0.45(f_i)^{0.55} \tag{10b}$$

Furthermore, according to Fig. 12b similar trends were identified between the particle indexes and the shear strength of brick–mortar joints made with LCM mortars. Equation (11a) and (11b) exhibits the relationships derived with the R-squared values of 0.6128 and 0.5389, respectively.

$$\tau_s = 0.11(f_A)^{1.48} \tag{11a}$$

$$\tau_s = 0.20(f_i)^{0.40} \tag{11b}$$

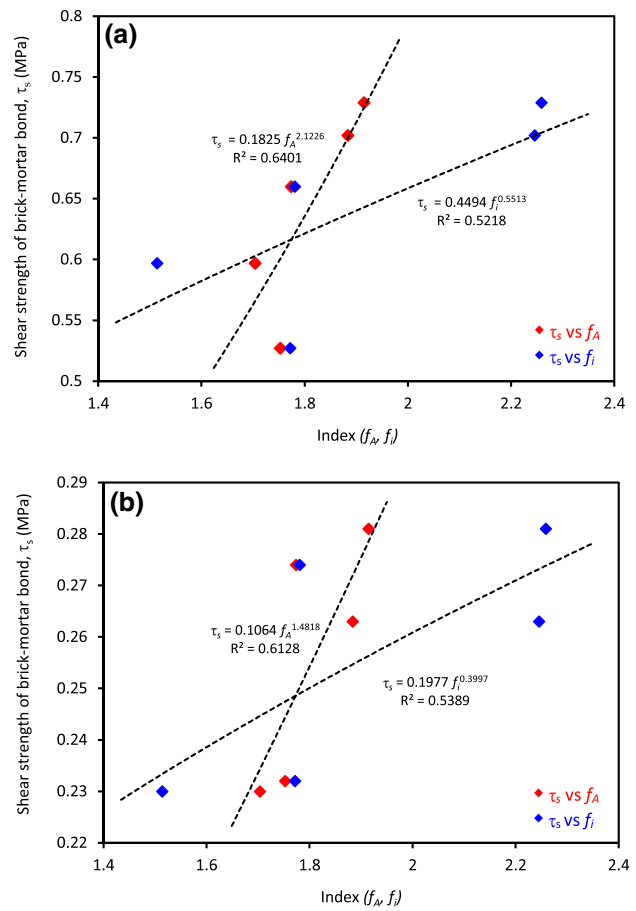


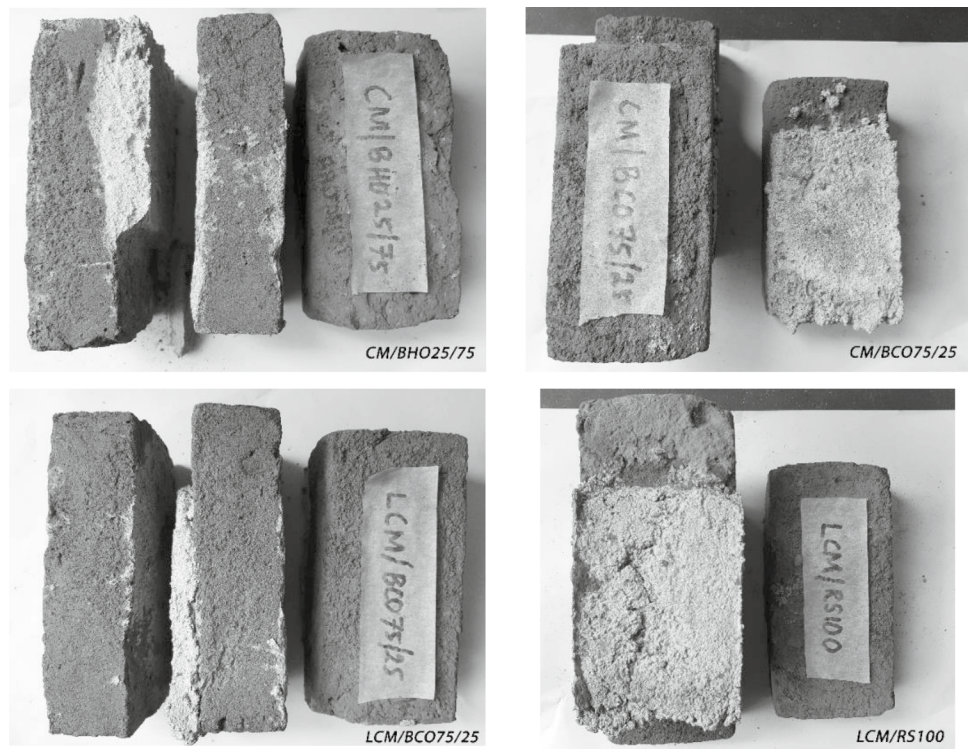
**Fig. 12** Effect of fine aggregate properties on shear bond strength–triplet specimens made with **a** CM mortars and **b** LCM mortars

From the above linear models, it is distinct that the fine aggregate physical characteristics such as angularity and surface roughness significantly impacted the shear bond strength of brick–mortar joint. Various shapes and surface textures may advance the slipping resistance between the particles, which could be the rationale for the significant effects in the present study. Here, it should be noted that both CM and LCM mortars revealed the similar shear bond strengths of brick–mortar joint when the angularity and surface roughness indexes of fine aggregates are equal. This could be because of the combined similar effects of shape and surface texture of particles. However, beyond this intersecting point the shear bond strength was significantly varied which highlights a pivotal role of the shape and surface characteristics of fine aggregates. This is one of the key observations from this study which requires a further investigation.

Figure 13 demonstrates the common failure types observed during the experiment. RILEM TC 127-MS-B.4 [62] recommends some characteristic failure patterns such as the failure at one or both unit/mortar interfaces, the failure of mortar and the failure of unit. Similarly, some triplet



**Fig. 13** Failure patterns of triplet samples under shear stress



**(a)** Both joints and mortar failure (top); Both joints failure only (bottom)

**(b)** Edge split with mortar (top); Edge split without mortar (bottom)

samples failed at both joints while a mortar failure was also noticed in some specimens in addition to the joint failure. In addition, the rest of the specimens manifested one joint failure.

**Adhesive bond stress–strain relationships and affecting parameters**

A very few studies have been executed on investigating the adhesive strength of brick–mortar bond, and this was achieved in this research by using cross-couplet specimens prepared with the defined mortars. There are no standard specifications available on determining the adhesive strength of brick–mortar joint. Hence, a laboratory setup was prepared to apply a direct tension stress on the specimen using a tensile testing machine with a capacity of 100 kN.

In the industrial applications, adhesiveness of brick–mortar joint is a crucial property in masonry constructions, which ensures the bonding capacity against tension. Table 8f shows the average adhesive strength of brick–mortar joint with each selected mortar. When mortars contained MS alone, the adhesive strength was increased than the RS100 mortar specimens. CM mortars such as MH100 and MC100 considerably increased the adhesive strength which were more than around 17% and 8%, respectively, than the control specimens. Regarding the bonding with LCM mortars, these values were observed as 4% and 11%.

Here, the mortars incorporated blended sands such as BHO25/75 and BCO75/25 manifested the highest adhesive strength than the other samples. The adhesive strength of brick–mortar joint was increased in the order of RS100 < MC100 < MH100 < BHO25/75 < BCO75/25. As shown in Fig. 6f, the stress–strain behavior of brick–mortar joint with each mortar was evolved with the tensile stress applied and then revealed a sudden failure. Moreover, the replacement of OPC with hydrated lime slightly reduced the adhesive strength of the brick–mortar joints.

The direct tension applied on the cross-couplet specimens depends on the total surface area of the joint. It is very important to investigate the effective contact area of brick and mortar at the joint when different fine aggregates are included. The uniform particle size distribution of fine aggregates enhances higher packing density of mortars by reducing the porosity and thus increases the total specific surface (refer to Fig. 5). Different gradation curves as illustrated in Fig. 2 were expected to affect the adhesiveness of the brick–mortar bonds. So, a relationship between the packing density of fine aggregates and the adhesive strength of brick–mortar joint was evaluated and is presented in Fig. 14. Equation 12 reveals an acceptable correlation between the adhesive strength of brick–mortar bond and the packing density of fine aggregate ( $\rho$ ) with the R-squared value of 0.7825.

$$\delta_A = 3 \times 10^{-9} \rho^{2.28} \tag{12}$$

During the testing, several failure types were observed, and the most identified patterns are illustrated in Fig. 15. As reported before, the mortar constituents did not influence the failure patterns. When the specimens reached the maximum tension stress, both brick and joint failure were observed. Considering the failure of bricks, generally bricks were fractured in either perpendicular (Fig. 15a) or parallel (Fig. 15c) to the joints. The types of mortar failure are identified in Fig. 15b, d.

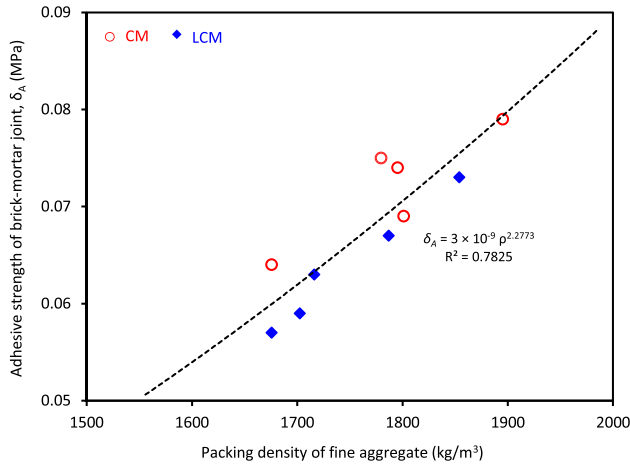
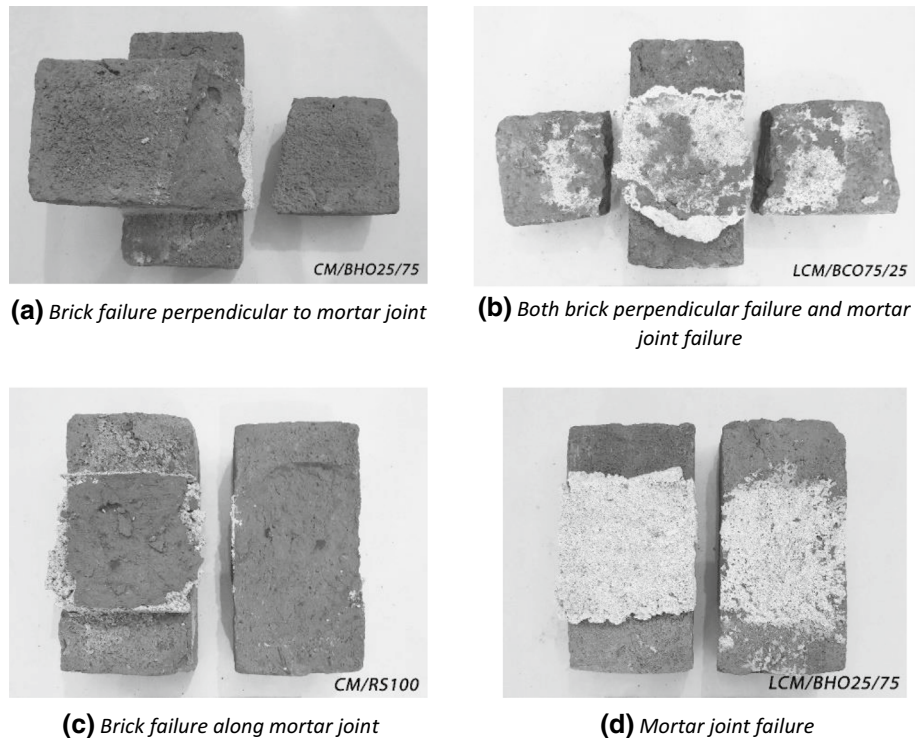


**Fig. 14** Effect of packing density of fine aggregate properties on adhesive bond strength

**Fig. 15** Common failure of cross-couplet samples under adhesive load (direct tension)



## Conclusions

Considerable studies have been executed on masonry with the effects of mortar properties. However, none of the studies are available on the influence of RS alternatives, which is the novelty of the present study. RS in CM and LCM mortars was fully replaced with MS and blending of MS and OS. Compressive strength, diagonal tensile strength and flexural strength of masonry were evaluated. Furthermore, shear bond strength and adhesive strength of brick-mortar joint were also investigated.

Masonry with CM and LCM mortars contained MS alone significantly advanced the compressive strength and the blended sand mortars also improved the strength. A linear model was developed concerning the compressive strength of masonry, compressive strength of mortar, angularity and surface roughness which is not available in the past studies.

The alternatives in CM mortars except MS alone increased the diagonal tensile strength of masonry. LCM mortars with the blended sands considerably decreased the strength than RS mortar. This is a good outcome as a very few studies are reporting the tensile behavior of masonry.

Each alternative in CM and LCM mortars considerably improved the flexural strength of masonry. The highest modulus of rupture was observed when mortars contained MS alone. A good correlation was noticed between the modulus of rupture of masonry and flexural strength of mortar which has not been reported in the past studies.

The mortars incorporated MS alone revealed inflated shear bond strength of brick–mortar joint and some improvements were noticed with blended sand mortars. The particle angularity and surface roughness showed a significant influence on the shear bond strength based on the good linear correlations.

Both CM and LCM mortars with the selected alternatives marginally surpassed the adhesive strength of brick–mortar joint than RS mortars. The reliance of adhesive bond strength on the packing density of fine aggregates manifested a positive correlation which can be incorporated in future investigations.

Because of the positive performance of masonry and brick–mortar joint, the selected alternatives are viable solutions to immediately cease the RS mining and thus the environmental and ecological impacts.

**Acknowledgements** The authors wish to acknowledge the INSEE Siam City, Sri Lanka, for providing necessary binding materials for conducting this study. Also, the authors wish to thank the technical staffs of the Department of Civil Engineering, University of Sri Jayewardenepura for granting necessary supports for carrying out the laboratory works.

## Declarations

**Conflict of interest** The authors declare that they have no conflict of interest.

## References

- McKenzie WMC (2001) Design of structural masonry, 1st edn. Palgrave Publishers Ltd., New York
- Singh SB, Munjal P (2017) Bond strength and compressive stress-strain characteristics of brick masonry. *J Build Eng* 9:10–16. <https://doi.org/10.1016/j.jobe.2016.11.006>
- Arya C (2009) Design of structural elements, 3rd edn. Taylor and Francis, Oxford shire
- Hendry AW, Sinha BP, Davies SR (2004) Design of masonry structures, 3rd edn. E & FN Spon, an imprint of Chapman & Hal, London
- Kosmatka SH, Wilson ML (2011) Aggregates for concrete. In: Design and control of concrete mixtures, 5th edn. Portland Cement Association (PCA), IL, pp 95–116
- Pereira K, Ratnayake R (2013) Water integrity in action. In: Curbing illegal sand mining in Sri Lanka. Water Integrity Network. [https://www.waterintegritynetwork.net/wp-content/uploads/2015/04/Case\\_SriLanka\\_SandMining\\_EN\\_2013.pdf](https://www.waterintegritynetwork.net/wp-content/uploads/2015/04/Case_SriLanka_SandMining_EN_2013.pdf). Accessed 16 Mar 2021
- Arulmoly B, Konthesingha C (2021) Pertinence of alternative fine aggregates for concrete and mortar: a brief review on river sand substitutions. *Aust J Civ Eng*. <https://doi.org/10.1080/14488353.2021.1971596>
- Gavrilitea MD (2017) Environmental impacts of sand exploitation. *Anal Sand Mark Sustain* 9(1118):1–26. <https://doi.org/10.3390/su9071118>
- Padmalal D, Maya K (2014) Sand mining: the world scenario. In: Sand mining, pp 57–80. [https://doi.org/10.1007/978-94-017-9144-1\\_5](https://doi.org/10.1007/978-94-017-9144-1_5)
- Koehnken L, Rintoul MS, Goichot M, Tickner D, Loftus AC, Acreman MC (2020) Impacts of riverine sand mining on freshwater ecosystems: a review of the scientific evidence and guidance for future research. *River Res Appl* 36:362–370. <https://doi.org/10.1002/rra.3586>
- Gonçalves JP, Tavares LM, Toledo Filho RD, Fairbairn EMR, Cunha ER (2007) Comparison of natural and manufactured fine aggregates in cement mortars. *Cem Concr Res* 37:924–932. <https://doi.org/10.1016/j.cemconres.2007.03.009>
- Cortes DD, Kim HK, Palomino AM, Santamarina JC (2008) Rheological and mechanical properties of mortars prepared with natural and manufactured sands. *Cem Concr Res* 38:1142–1147. <https://doi.org/10.1016/j.cemconres.2008.03.020>
- Guifeng L, Shichao L, Zhengfa C, Yanlong Q (2014) Effect of different grain grading of manufactured sands on properties of dry-mixed mortar. *Appl Mech Mater* 507:429–433. <https://doi.org/10.4028/www.scientific.net/AMM.507.429>
- Aoual-Benslafa FK, Kerdal D, Ameer M, Mekerta B, Semcha A (2015) Durability of mortars made with dredged sediments. *Proc Eng* 118:240–250. <https://doi.org/10.1016/j.proeng.2015.08.423>
- De Schutter G, Poppe AM (2004) Quantification of the water demand of sand in mortar. *Constr Build Mater* 18:517–521. <https://doi.org/10.1016/j.conbuildmat.2004.04.004>
- Manjunath BTA, Karthick TR, Manjunath MS, Lakshmi K (2017) Partial replacement of sea and desert sand in place of river sand for mortar in construction. *Glob Res Dev J Eng* 2(7):81–85
- Malyszko L (2005) In-plane shear and tensile strength tests of small brickwork specimens. In: Structural analysis of historical constructions. London: Taylor & Francis Group, pp 291–298. <http://www.hms.civil.uminho.pt/sahc/2004/291.pdf>. Accessed 14 Dec 2020
- Costigan A, Pavia S, Kinnane O (2015) An experimental evaluation of prediction models for the mechanical behavior of unreinforced, lime-mortar masonry under compression. *J Build Eng* 4:283–294. <https://doi.org/10.1016/j.jobe.2015.10.001>
- Dehghan SM, Najafgholipour MA, Baneshi V, Rowshanzamir M (2018) Mechanical and bond properties of solid clay brick masonry with different sand grading. *Constr Build Mater* 174:1–10. <https://doi.org/10.1016/j.conbuildmat.2018.04.042>
- Pavia S, Hanley R (2010) Flexural bond strength of natural hydraulic lime mortar and clay brick. *Mater Struct* 43:913–922. <https://doi.org/10.1617/s11527-009-9555-2>
- Thaickavil NN, Thomas J (2018) Behavior and strength assessment of masonry prisms. *Case Stud Constr Mater* 8:23–38. <https://doi.org/10.1016/j.cscm.2017.12.007>
- Sarangapani G, Venkatarama Reddy BV, Jagadish KS (2005) Brick-mortar bond and masonry compressive strength. *J Mater Civ Eng* 17(2):229–237. [https://doi.org/10.1061/\(ASCE\)0899-1561\(2005\)17:2\(229\)](https://doi.org/10.1061/(ASCE)0899-1561(2005)17:2(229))
- Singhal V, Rai DC (2014) Suitability of half-scale burnt clay bricks for shake table tests on masonry walls. *J Mater Civ Eng* 26(4):644–657. [https://doi.org/10.1061/\(ASCE\)MT.1943-5533.0000861](https://doi.org/10.1061/(ASCE)MT.1943-5533.0000861)
- Konthesingha KMC, Jayasinghe C, Nanayakkara SMA (2007) Bond and compressive strength of masonry for locally available bricks. *Engineer* 40(4):7–13. <https://doi.org/10.4038/engineer.v40i4.7148>
- Griffith MC, Lam NTK, Wilson JL, Doherty K (2004) Experimental investigation of unreinforced brick masonry wall in flexure. *J Struct Eng* 130(3):423–432. [https://doi.org/10.1061/\(ASCE\)0733-9445\(2004\)130:3\(423\)](https://doi.org/10.1061/(ASCE)0733-9445(2004)130:3(423))
- Ghazy MF (2012) Effect of using mortar interface and overlays on masonry behavior by using taguchi method. *ACI Mater J* 109(5):509–516
- Ghazy MF (2020) Optimization of recycled concrete aggregate geopolymer bricks by Taguchi method. *Revista De La*



- Construcción. *J Constr* 19(2):244–254. <https://doi.org/10.7764/rdlc.19.2.244-254>
28. Arulmoly B, Konthesingha C, Nanayakkara A (2021) Performance evaluation of cement mortar produced with manufactured sand and offshore sand as alternatives for river sand. *Constr Build Mater*. <https://doi.org/10.1016/j.conbuildmat.2021.123784>
  29. Arulmoly B, Konthesingha C, Nanayakkara A (2021) Effects of blending manufactured sand and offshore sand on rheological, mechanical and durability characterization of lime–cement masonry mortar. *Eur J Environ Civ Eng*. <https://doi.org/10.1080/19648189.2021.1995506>
  30. Sing MCP, Love PED, Tam CM (2012) Review and exploration of river sand substitutes for concrete production in Asian countries In: *Advances in civil engineering and building materials*. CRC Press, London, pp 115–117
  31. Branavan A, Konthesingha KMC (2019) Fine aggregate usage in concrete and masonry mortar by local construction industries. In: *10th international conference on structural engineering and construction management (ICSECM)*, pp 106–113. <https://doi.org/10.5281/zenodo.4136782>
  32. British Standard Institution (2000) EN 197–1: Cement—Part 1: composition, specifications and conformity criteria for common cements
  33. Sri Lanka Standards Institute (2015) SLS 107: Sri Lanka Standard Specification for Ordinary Portland Cement, 5th ed
  34. ASTM International (2018) ASTM C207-18: Standard specification for hydrated lime for masonry purposes. In: *Annual Book of ASTM Standards*
  35. ICTAD (2004) ICTAD Publication No: SCA/4/1—Specifications for building works—vol. I. Ministry of Housing and Construction, 3rd ed
  36. ASTM International (2018) ASTM C144-18: Standard specification for aggregate for masonry mortar. In: *Annual Book of ASTM Standards*
  37. ASTM International (2019) ASTM C294-19: Standard descriptive nomenclature for constituents of concrete aggregates. In: *Annual Book of ASTM Standards*
  38. Branavan A, Konthesingha KMC, Nanayakkara SMA, Premasiri HMR (2020) Optimizing blending of manufactured sand with offshore sand based on physical and virtue characteristics. *J Mater Sci Res Rev* 6(3):11–31
  39. British Standard (1992) BS 882: Specification for aggregates from natural sources for concrete. British Standards Institute
  40. British Standard (1997) BS 5328: Concrete—Part 1. Guide to specifying concrete. British Standards Institute
  41. British Standard (2016) BS EN 998-2: specification for mortar for masonry. Masonry mortar. British Standards Institute
  42. Dias W, Seneviratne G, Nanayakkara S (2008) Offshore sand for reinforced concrete. *Constr Build Mater* 22:1377–1384. <https://doi.org/10.1016/j.conbuildmat.2007.04.006>
  43. ASTM International (2015) ASTM C128-15: Standard test method for density, relative density (specific gravity) and absorption of fine aggregate. In: *Annual book of ASTM Standards*. West Conshohocken: American Society for Testing and Materials
  44. ASTM International (2017) ASTM C117-17: Standard test method for materials finer than 75- $\mu\text{m}$  (No. 200) sieve in mineral aggregates by washing. In: *Annual book of ASTM Standards*. West Conshohocken: American Society for Testing and Materials
  45. ASTM International (2017) ASTM C29/C29M-17a: Standard test method for bulk density (“unit weight”) and voids in aggregate. In: *Annual book of ASTM standards*. West Conshohocken: American Society for Testing and Materials
  46. ASTM International (2017) ASTM C1252-17: Standard test methods for uncompacted void content of fine aggregate (as influenced by particle shape, surface texture, and grading). In: *Annual Book of ASTM Standards*. West Conshohocken: American Society for Testing and Materials
  47. ASTM International (2020) ASTM C70–20: standard test method for surface moisture in fine aggregate. In: *Annual book of ASTM standards*. West Conshohocken: American Society for Testing and Materials
  48. ASTM International (2017) ASTM C142/C142M-17: standard test method for clay lumps and friable particles in aggregates. In: *Annual book of ASTM standards*. West Conshohocken: American Society for Testing and Materials
  49. Murdock L (1960) The workability of concrete. *Mag Concr Res* 12(36):135–144. <https://doi.org/10.1680/mac.1960.12.36.135>
  50. ASTM International (2006) ASTM D3398-00: Standard test method for index of aggregate particle shape and texture. In: *Annual Book of ASTM Standards*. West Conshohocken: American Society for Testing and Materials
  51. ASTM International (2020) ASTM C67/C67M-20: standard test methods for sampling and testing brick and structural clay tile. In: *Annual Book of ASTM Standards*. West Conshohocken: American Society for Testing and Materials
  52. ASTM International (2019) ASTM C270-19ae1: standard specification for mortar for unit masonry. In: *Annual Book of ASTM Standards*. West Conshohocken: American Society for Testing and Materials
  53. British Standard (2004) EN 1015-3: Methods of test for mortar for masonry—Part 3: determination of consistence of fresh mortar (by flow table). British Standards Institute
  54. British Standard (2007) EN 1015-11: Methods of test for mortar for masonry—Part 11: Determination of flexural and compressive strength of hardened mortar. British Standards Institute
  55. ASTM International (2018) ASTM C531-18: Standard test method for linear shrinkage and coefficient of thermal expansion of chemical-resistant mortars, grouts, monolithic surfacings, and polymer concretes. In: *Annual Book of ASTM Standards*
  56. Navaratnarajah S, Rumeskumar U (2018) Effect of moisture condition on mechanical behavior of low strength brick masonry. *J Build Eng* 17:23–31. <https://doi.org/10.1016/j.job.2018.01.015>
  57. Sahu S, Teja PRR, Sarkar P, Davis R (2019) Effect of brick prewetting on masonry bond strength. *J Mater Civ Eng* 31(10):1–9. [https://doi.org/10.1061/\(ASCE\)MT.1943-5533.0002866](https://doi.org/10.1061/(ASCE)MT.1943-5533.0002866)
  58. Haach VG, Vasconcelos G, Lourenço PB (2014) Assessment of compressive behavior of concrete masonry prisms partially filled by general mortar. *J Mater Civ Eng* 26. [https://doi.org/10.1061/\(ASCE\)MT.1943-5533.0000956](https://doi.org/10.1061/(ASCE)MT.1943-5533.0000956)
  59. ASTM International (2018) ASTM C1314-18: standard test method for compressive strength of masonry prisms. In: *Annual Book of ASTM Standards*
  60. ASTM International (2020) ASTM E519/E519M-20: standard test method for diagonal tension (shear) in masonry assemblages. In: *Annual Book of ASTM Standards*
  61. ASTM International (2015) ASTM E518/E518M-15: standard test methods for flexural bond strength of masonry. In: *Annual Book of ASTM Standards*
  62. RILEM TC 127-MS (1996) MS-B.4: Determination of shear strength index for masonry unit/mortar junction. In: *Tests for masonry materials and structures, materials and structures*, vol 29, pp 459–475. <https://www.rilem.net/images/publis/119203.pdf>. Accessed 05 Feb 2021
  63. ASTM International (2018) ASTM C952-12: standard test method for bond strength of mortar to masonry units (withdrawn 2018). In: *Annual Book of ASTM Standards*